Chinese Chemical Letters 37 (2026) 112051

Contents lists available at ScienceDirect

Chinese Chemical Letters

journal homepage: www.elsevier.com/locate/cclet

Dovetail joint strategy for constructing giant multi-propeller supramolecular architectures

He Zhao[b,c], Qiangqiang Dong[b], Fengxue Liu[b], Ning Wang[a], Lijun Wang[a], Mingzhao Chen[a], Zhilong Jiang[a], Die Liu[b], Jun Wang[a,**], Pingshan Wang[a,b,*], Yiming Li[b,*]

[a] Institute of Environmental Research at Greater Bay Area, Key Laboratory for Water Quality and Conservation of the Pearl River Delta, Ministry of Education, Guangzhou Key Laboratory for Clean Energy and Materials, Guangzhou University, Guangzhou 510006, China
[b] Department of Organic and Polymer Chemistry, Hunan Key Laboratory of Micro & Nano Materials Interface Science, College of Chemistry and Chemical Engineering, Central South University, Changsha 410083, China
[c] School of Chemistry and Materials Engineering, Fuyang Normal University, Fuyang 236037, China

ARTICLE INFO

Article history:
Received 8 August 2025
Revised 26 October 2025
Accepted 31 October 2025
Available online 31 October 2025

Keywords:
Terpyridine
Self-assembly
Mortise-and-tenon ligands
Dovetail joint strategy
Propeller supramolecules

ABSTRACT

The structural principles of traditional Chinese mortise-and-tenon joints have inspired breakthroughs in supramolecular engineering. Nevertheless, substantial challenges remain in constructing nanoscale supramolecular architectures with precisely controlled giant dimensions. Herein, we report a precision-guided synthetic strategy for constructing giant 2D and 3D supramolecular architectures with rhomboidal motifs, which was achieved through a dovetail joint strategy. Initial assembly of bis-mortise ligand **L1** with dovetail tenon ligand **L2** in the presence of Cd^{2+} ions yielded the fundamental bis-rhombic supramolecule **R1**. Subsequent structural elaboration of the dovetail tenon motif enabled the development of multitopic ligands **L3** and **L4**, which facilitated the construction of expanded architectures of the giant bis-propeller supramolecule **R2** and tris-propeller supramolecule **R3**. The synthesized supramolecules **R1–R3** were fully characterized multidimensional NMR spectroscopy, electrospray ionization mass spectrometry (ESI-MS), traveling wave ion mobility mass spectrometry (TWIM-MS), transmission electron microscopy (TEM), and atomic force microscopy (AFM). This work develops an innovative dovetail-joint assembly strategy for constructing rigid giant supramolecular architectures, establishing a new paradigm for precision engineering of complex 3D molecular systems.

© 2025 Published by Elsevier B.V. on behalf of Chinese Chemical Society and Institute of Materia Medica, Chinese Academy of Medical Sciences.

Coordination-driven self-assembly represents a highly effective approach for spontaneous formation of well-defined supramolecular architectures with precisely controlled geometries and topologies [1–11]. This approach leverages straightforward mixing procedures and precise condition tuning, thereby circumventing intricate chemical reaction pathways. By judiciously selecting diverse metal ions and building blocks, or fine-tuning reaction parameters (including solvent type, temperature, and concentration), it empowers researchers to exert meticulous control over the resultant product's structural morphology [12–17]. These metal-organic supramolecular assemblies featuring various metal ions and functionalizable organic ligands, exhibit diverse physical and chemical properties and possess significant application values in fields such as catalysis, sensing, and drug delivery [18–24]. However, as the complexity of ligands and target assembly products increases, achieving precise regulation at the nanoscale through non-covalent interactions remains a key scientific problem in this field [25–31].

The mortise-and-tenon joint is a Chinese traditional woodworking technique that integrates superb craftsmanship aesthetics and practicality [32–34]. Such joints consist of tenons (protruding parts) and corresponding mortises (recessed parts). Tenons, usually in unique trapezoidal or wedge shapes, precisely interlock with mortises [32]. This modular and structurally interlocking design endows the joints with excellent stability. Such joints are composed of two complementary components: tenons as the protruding parts and mortises as the recessed parts. The tenons, often shaped as distinctive trapezoids or wedges, fit precisely into the mortises to create a secure interlock, endowing the overall architecture remarkable stability [32,35]. In the design and construction of supramolecular structures, a similar design principle is also applicable to enhance the stability by precisely designing the

* Corresponding authors at: Department of Organic and Polymer Chemistry, Hunan Key Laboratory of Micro & Nano Materials Interface Science, College of Chemistry and Chemical Engineering, Central South University, Changsha 410083, China.
** Corresponding author.
E-mail addresses: wangjun@gzhu.edu.cn (J. Wang), chemwps@csu.edu.cn (P. Wang), chemyl@csu.edu.cn (Y. Li).

https://doi.org/10.1016/j.cclet.2025.112051
1001-8417/© 2025 Published by Elsevier B.V. on behalf of Chinese Chemical Society and Institute of Materia Medica, Chinese Academy of Medical Sciences.

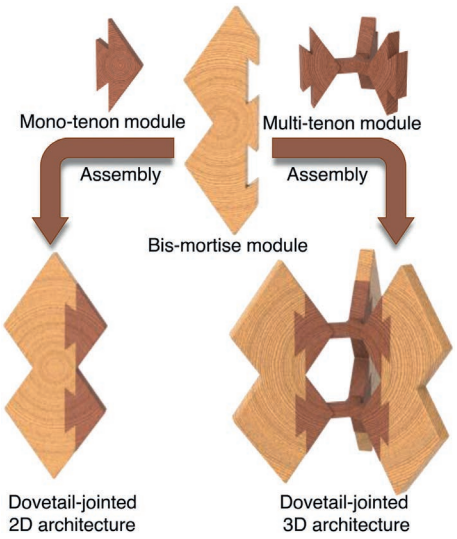


Fig. 1. Cartoon illustration of dovetail joints in construction of architecture.

geometric arrangement of intermolecular interactions, such as hydrogen bonds, coordination bonds, and other non-covalent forces [36–41]. Therefore, the design principle of mortise-and-tenon joints provides new ideas and strategic references for constructing complex and stable supramolecular structures.

The dovetail joint, a type of mortise-and-tenon structure, is composed of a tenon-shaped like a swallow's tail and a corresponding mortise. It can generate strong tensile resistance and stability due to its unique geometric structure and is widely used in the structural connections of wooden boxes, furniture, and ancient buildings (Fig. 1) [42,43]. Herein, we successfully constructed three rhombic supramolecular structures of increasing complexity by drawing on the design concept of dovetail joints. Through a stepwise synthesis method [44–46], a W-shaped multidentate metallo-organic ligand **L1** was designed and prepared as the mortise (Fig. 2a). In the presence of Cd^{2+} ions, **L1** was combined with the geometrically complementary V-shaped dovetail tenon ligand **L2**, successfully obtaining fundamental bis-rhombic supramolecule **R1** (Fig. 2b). Different from previously reported rhombic structures, **R1** connects two rhombic units *via* a central benzene ring. The subsequent elucidation of the dovetail motif structure led to the development of ligands **L3** and **L4**, containing multiple tenons. These ligands enabled the construction of larger-scale extended architectures, specifically the bis-propeller-shaped supramolecule **R2** and the tris-propeller-shaped supramolecule **R3** (Fig. 2b). **R2** and **R3** incorporate two and three **R1** structural units, respectively. These units were coupled by bridging ligands extended from the central tenon ligands, further facilitating the construction of giant supramolecular structures.

The critical W-shaped bis-mortise ligand **L1** was synthesized in a stepwise manner, and the final step was a four-fold Suzuki-coupling between tetra–bromo complex **9** and boronic ester **10**. **L1** incorporates four free terpyridine (tpy) units, each bearing bulky groups at the 6-position to promote heteroleptic coordination with ordinary tpy units (Scheme S1 in Supporting information) [47,48]. The ^{1}H NMR spectrum of **L1** (Fig. 3a and Fig. S25 in Supporting information) showed two partially overlapping resonances at 9.12 and 9.00 ppm with an integration ratio of 1:1. These are assigned to four kinds distinct $H^{3',5'}$ protons from the Ru^{2+}-coordinated tpy units (two pairs accidentally overlapping). In the non-aromatic region, five singlets at 4.10, 3.71, 3.70, 3.17, and 3.02 ppm were observed with an integration ratio of 2:8:8:1:1, corresponding to five types of $-OCH_3$ protons. All other protons were assigned based on 2D COSY and 2D NOESY NMR experiments (Figs. S26 and S27 in Supporting information) [49,50]. To confirm the molecular structure of ligand **L1**, high-resolution ESI-MS was conducted [51–53]. The ESI-MS spectrum exhibits five prominent signals at *m/z* 761.63, 910.46, 1108.89, 1386.70, and 1803.41, with isotope patterns matching the calculated distributions, corroborating the successful synthesis of **L1** (Fig. S57 in Supporting information).

The V-shaped dovetail tenon ligand **L2** was next prepared in one step by Suzuki coupling 3,5-dibromoanisole with 4′-(4-boronatophenyl)-2,2′:6′,2′′-terpyridine (Scheme S1 in Supporting information) [54–56]. A mixture of **L2**, the W-shaped bis-mortise ligand **L1** and $Cd(NO_3)_2$ (2:1:4 molar ratio) in $CHCl_3/CH_3CN$ (v/v, 1/2) was stirred at 70 °C for 12 h. After cooling to the room temperature, excess saturated methanolic $LiNTf_2$ was added to exchange counter-anions, giving the red precipitate **R1** in nearly quantitative yield (97 %). The composition of assembled product **R1** was unambiguously ensured by NMR and MS analysis. As shown in Fig. 3a, the ^{1}H NMR spectrum of **R1** exhibited one set of overlapping aromatic signals (9.15–9.13 ppm) and three singlets (9.09, 9.07, and 9.04 ppm), corresponding to the eight magnetically distinct $H^{3',5'}$ protons of the tpy moieties. In the non-aromatic region, two overlapped signal peaks (4.27–4.24 ppm and 2.89 ppm) and four well-resolved singlets (4.14, 4.11, 3.33, and 3.32 ppm) were observed, with an integral ratio of 8:48:6:6:3:3, consistent with two kinds of $-OCH_2-$ protons and six kinds of $-OCH_3$ protons (Fig. S37 in Supporting information). Notably, the $H^{6,6''}$ protons of the tpy moiety in **R1** exhibited a pronounced upfield shift compared to free ligand **L2** [57,58], attributed to electron shielding effects upon coordination with Cd^{2+}, thereby confirming the successful assembly of **L1**, **L2**, and Cd^{2+}. The remaining assignments were verified by 2D COSY and 2D NOESY spectra (Figs. S38 and S39 in Supporting information).

ESI-MS and TWIM-MS analyses were carried out to determine the exact composition of **R1**. As shows in Fig. 3b, the ESI-MS spectrum exhibits a series of continue charge states from 6+ to 14+ at *m/z* 1798.72, 1501.62, 1278.89, 1105.41, 967.09, 853.70, 759.21, 679.19, and 610.61, arising from sequential loss of NTf_2^- counterions. Deconvolution of the ESI-MS data gives a molecular weight of 12,472 Da for **R1**, in excellent agreement with the theoretical value calculated for $\mathbf{[(Cd_4L1L2_2)(NTf_2^-)_{16}]}$, thereby confirming the successful formation of the targeted bis-rhombic supramolecule. Moreover, the isotope patterns for all charge states are in excellent agreement with simulations (Fig. S61 in Supporting information). The TWIM-MS plot shows a narrow drift-time distribution for each charge state from 8+ to 13+, confirming the exclusive presence of the target discrete structure and the absence of other isomers (Fig. 3b).

Building on the successful construction of the bis-rhombic supramolecule **R1** *via* the dovetail joint strategy, we redesigned a structurally expanded bis-tenon ligand to further assemble propeller-shaped supramolecules featuring united bis-rhombus motifs. The corresponding metallo-organic ligand **L3**, bearing the requisite dual-dovetail modules, was then rationally designed and synthesized *via* an analogous stepwise method (Scheme S2, Figs. S31-S33 and S59 in Supporting information).

Upon addition of ligands **L1**, **L3** and $Cd(NO_3)_2$ in CH_3CN/CH_3OH (v/v, 1/1) in a 1:1:4 stoichiometric ratio, the mixture was refluxed for 8 h (Scheme S5 in Supporting information). After adding an excess methanolic solution of $LiNTf_2$ to exchange the counter-anions, a red precipitate, **R2**, was obtained in nearly quantitative yield (97 %). NMR spectroscopy was preliminarily used to provide structural information. As shown in Fig. 3c, the aromatic region displays one overlapping multiplet (9.03–9.02 ppm) and four singlets (9.06, 8.97, 8.96, and 8.94 ppm) assigned to the nine kinds of tpy-$H^{3',5'}$ protons. Signals for the $-OCH_3$ and $-OCH_2-$ groups in the non-aromatic region are also consistent with the expected

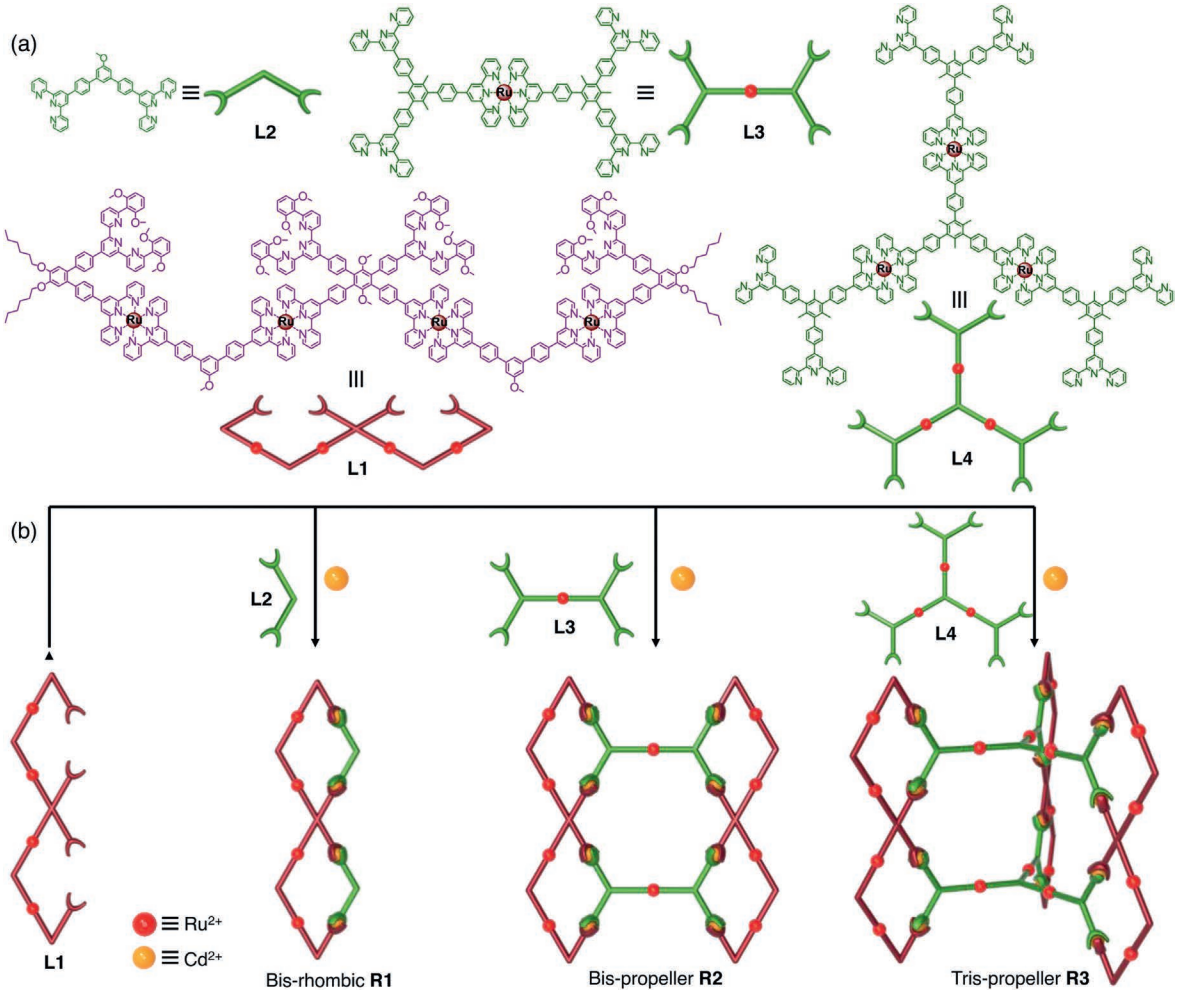


Fig. 2. Mortise-and-tenon type ligands and their self-assembly. (a) Mortise-shaped building blocks **L1** and tenon-shaped building blocks **L2**-**L4**. (b) Self-assembly of bis-rhombic supramolecule **R1**, bis-propeller supramolecule **R2**, and tris-propeller supramolecule **R3**.

structure (Fig. 3c and Fig. S41 in Supporting information). Compared with **L3**, the tpy-$H^{6,6''}$ protons of **R2** are shifted upfield because of the electron-shielding effect, confirming successful combination of **L1** and **L3** with Cd^{2+}. All other resonances were unambiguously assigned with the aid of 2D COSY and NOESY analyses (Figs. S42 and S43 in Supporting information). Here, the collective data support the successful assembly of the intended bis-propeller supramolecule.

To confirm the successful assembly of the bis-propeller supramolecule, ESI-MS and TWIM-MS analyses were further performed. The ESI-MS spectrum displayed a continuous series of charge states from 13+ to 23+, generated by sequential loss of NTf_2^- anions. The observed *m/z* values matched the theoretical isotope pattern calculated for $\mathbf{[(Cd_8L1_2L3_2)(NTf_2^-)_{36}]}$, corresponding to a molecular weight of 27,511 Da, thereby corroborating the formation of the target bis-propeller (Fig. 3d). TWIM-MS revealed a single, narrow drift-time distribution for charge states ranging from 15+ to 25+, confirming the sole exist of bis-propeller supramolecule **R2** and the absence of isomers or oligomers (Fig. 3d).

With the planar bis-propeller supramolecule **R2** in hand, we now aim to construct multi-propeller architectures and explore more complex three-dimensional tris-propeller systems. Herein, we designed a triple-dovetail metallo-organic ligand **L4**, constructed from three **L2** units interconnected *via* *a*⟨tpy-Ru^{2+}-tpy⟩ coordinated triangular scaffold, exhibiting a fractal-like dendritic architecture. The detailed synthetic procedures and comprehensive characterization data for ligand **L4** are provided in Figs. S34-S36 (Supporting information). Similarly, we employed the same strategy to assemble ligands **L1** and **L4** with $Cd(NO_3)_2$, yielding the supramolecular product **R3** in nearly quantitative yield (98%). Compared to **R1** and **R2**, **R3** displayed markedly reduced solubility in CD_3CN, requiring the addition of DMF-d_7 to obtain adequate sample concentrations for NMR spectroscopic analysis. The ^1H NMR spectra of **L1**, **R3**, and **L4** are comparatively displayed in Fig 4a. Notably, **R3** exhibits broadened signal peaks, consistent with the formation of a high-molecular-weight assembly. All proton resonances were unambiguously assigned using 2D COSY and NOESY spectroscopy (Figs. S46 and S47 in Supporting information). In contrast to ligand **L4**, assembly product **R3** displays significant upfield shifts for the characteristic tpy-$H^{6,6'}$ protons, confirming successful coordination to Cd^{2+} ions. The ESI-MS spectrum of **R3** exhibited a consecutive series of *m/z* peaks corresponding to 18+ to 32+ charge states, resulting from the progressive loss of NTf_2^- anions (Fig. 4c). Additional low-intensity peaks were attributed to adducts formed with two $LiNTf_2$ units (Figs. S63 and S64 in Supporting information). The experimental data showed excellent agreement with the theoretical values calculated for the tris-propeller supramolecule $\mathbf{[(Cd_{12}L1_3L4_2)(NTf_2^-)_{60}]}$ (Fig. 4b), which has a molecular mass of 45,380 Da. TWIM-MS analysis further confirmed the monodisperse nature of **R3**, as evidenced by a single narrow drift time distribution across the 23+ to 32+ charge

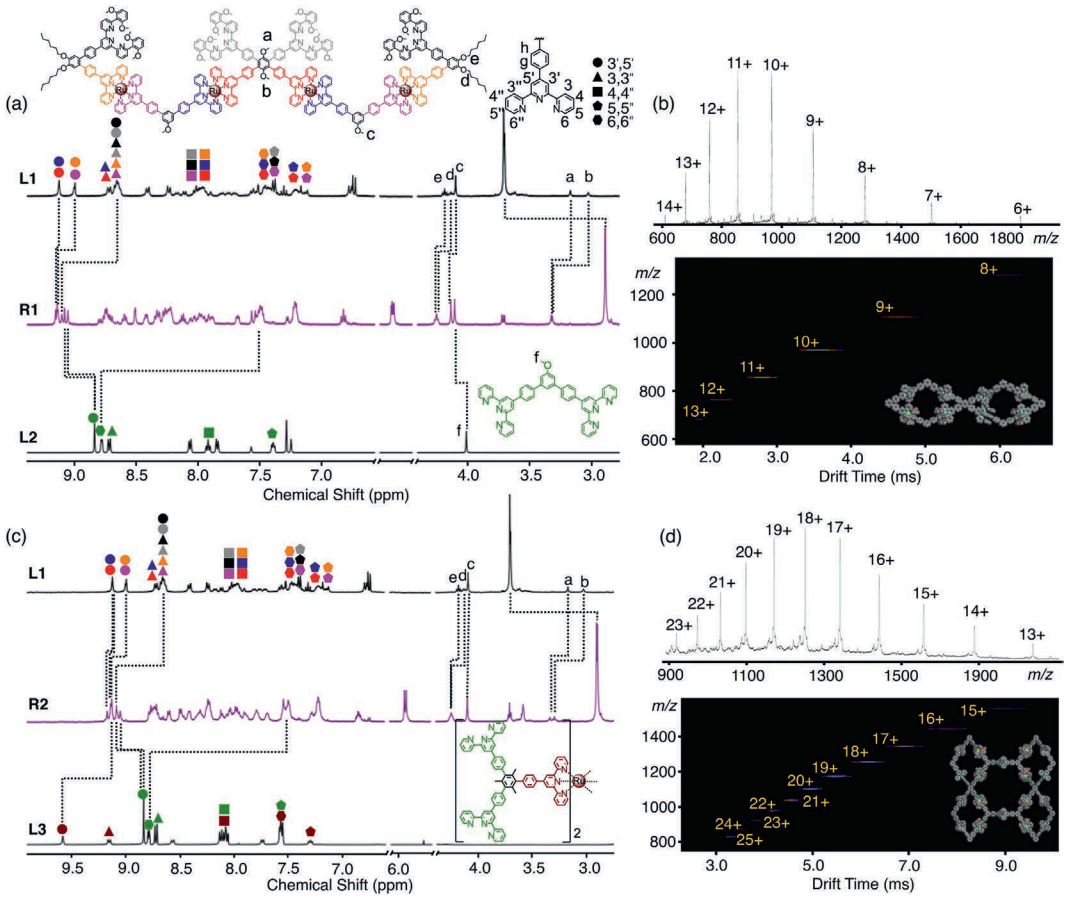


Fig. 3. ^{1}H NMR spectra (400 MHz, 298 K, CD_3CN) of (a) **L1**, **R1**, and **L2**, and (c) **L1**, **R2**, and **L3**. ESI-MS spectra and TWIM-MS plots of supramolecules (b) **R1** and (d) **R2**.

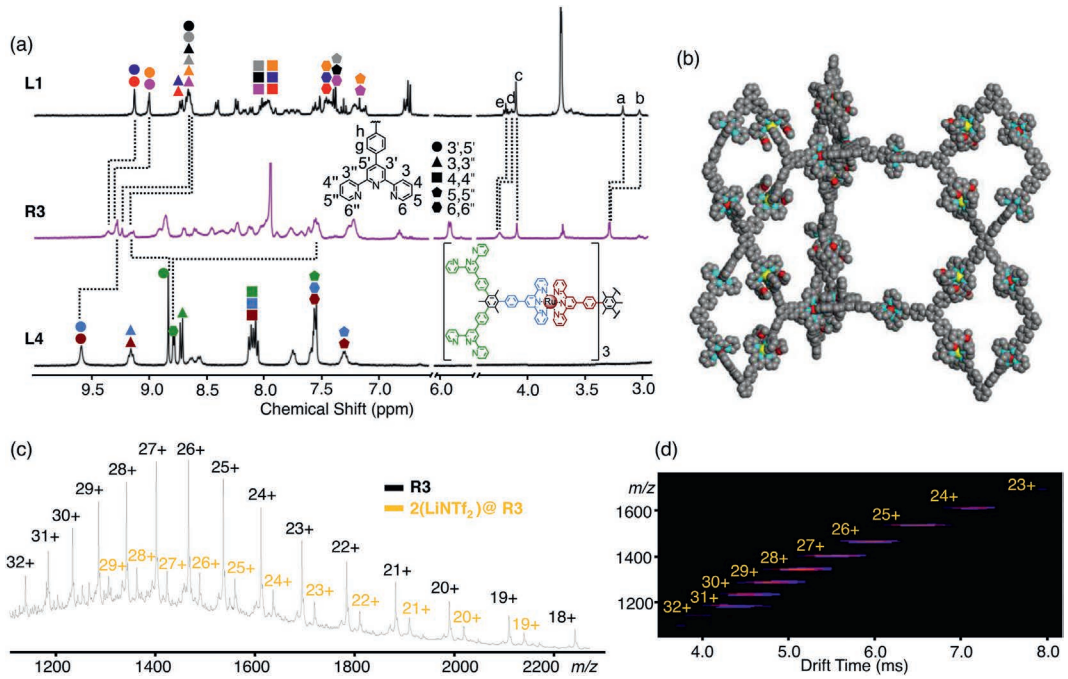


Fig. 4. ^{1}H NMR spectra (400 MHz, 298 K) of (a) **L1** in CD_3CN, **R3** in CD_3CN/DMF-d_7 (v/v, 4/1), and **L4** in CD_3CN. (c) Representative energy-minimized structures from molecular model of **R3**. (b) ESI-MS spectrum and (d) TWIM-MS plot of **R3**.

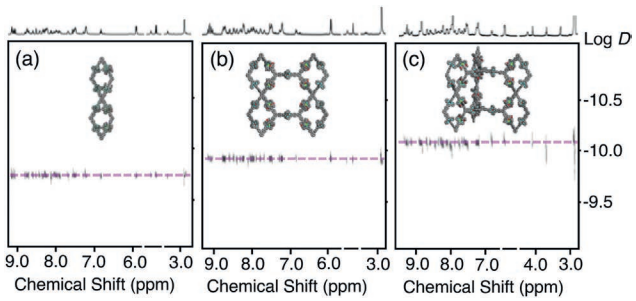


Fig. 5. DOSY spectra (500 MHz, 298 K) of (a) **R1** in CD_3CN, (b) **R2** in CD_3CN, and (c) **R3** in CD_3CN/DMF-d_7 (v/v, 4/1).

states (Fig. 4d). This observation definitively excludes the presence of isomeric or oligomeric species. Taken together, these comprehensive analytical results provide conclusive evidence for the successful assembly of the well-defined, tris-propeller supramolecule **R3**.

Numerous crystallization attempts were made for **R1-R3**, but only precipitates were obtained. To elucidate the detail size and height information of the assembly products, we employed diffusion-ordered spectroscopy (DOSY) and transmission electron microscopy (TEM) analysis to characterize the shape and size of **R1**-**R3**, while atomic force microscopy (AFM) was utilized for precise height measurements of **R3** [59–62]. As illustrated in Fig. 5, the DOSY experiments revealed three distinct bands with diffusion coefficients (Log*D*) of −9.74, −9.88, and −10.05 for **R1**-**R3**, respectively (Table S1 and Fig. S49 in Supporting information). These well-resolved signals clearly indicate the presence of discrete and well-defined species in solution. TEM characterization was performed on supramolecular assemblies **R1**-**R3** by drop-casting their CH_3CN solutions ($\sim 10^{-6}$ mol/L) onto carbon-coated copper grids (400 mesh). As evidenced in Figs. 6a-c, all three assemblies exhibited uniform dispersion on the carbon support. High-resolution imaging showed that **R1** exhibited dimensions comparable to its geometry-optimized structure, while **R2** and **R3** displayed well-defined nanoparticles with diameters of 8.1 ± 0.2 nm and 8.0 ± 0.2 nm, respectively (Fig. S66 in Supporting information). These measurements show excellent agreement with the predicted molecular dimensions from computational modeling (Figs. S67 and S68 in Supporting information), confirming the structural integrity of all three supramolecules in the solid state. AFM topographic imaging clearly resolved monodisperse **R3** assemblies on mica with a uniform height of 8.0 ± 0.2 nm (Figs. 6d and e), in excellent agreement with molecular modeling predictions (Fig. S68 in Supporting information). Collectively, these analytical results demonstrate the successful construction of three designed supramolecular architectures: the bis-rhombic **R1**, bis-propeller **R2**, and tris-propeller **R3**.

In summary, we have successfully constructed giant 2D and 3D supramolecular architectures through a bioinspired dovetail joint assembly strategy. Both the fundamental bis-rhombic **R1** and expanded bis-propeller **R2**/tris-propeller **R3** demonstrated precise structural control and exceptional stability *via* rationally designed multi-site ligands. Comprehensive characterization by NMR, ESI-MS, TWIM-MS, TEM, and AFM unequivocally confirmed the well-defined architectures of these supramolecular assemblies. The controlled structural evolution from simple building blocks to complex architectures revealed that enhanced binding interactions and spatial organization contribute significantly to structural integrity. This work provides a new approach for supramolecular engineering and paves the way for developing functional nanomaterials with practical applications.

Declaration of competing interest

We declare that we have no financial and personal relationships with other people or organizations that can inappropriately influence our work, there is no professional or other personal interest of any nature or kind in any product, service and/or company that could be construed as influencing the position presented in, or the review of, the manuscript entitled.

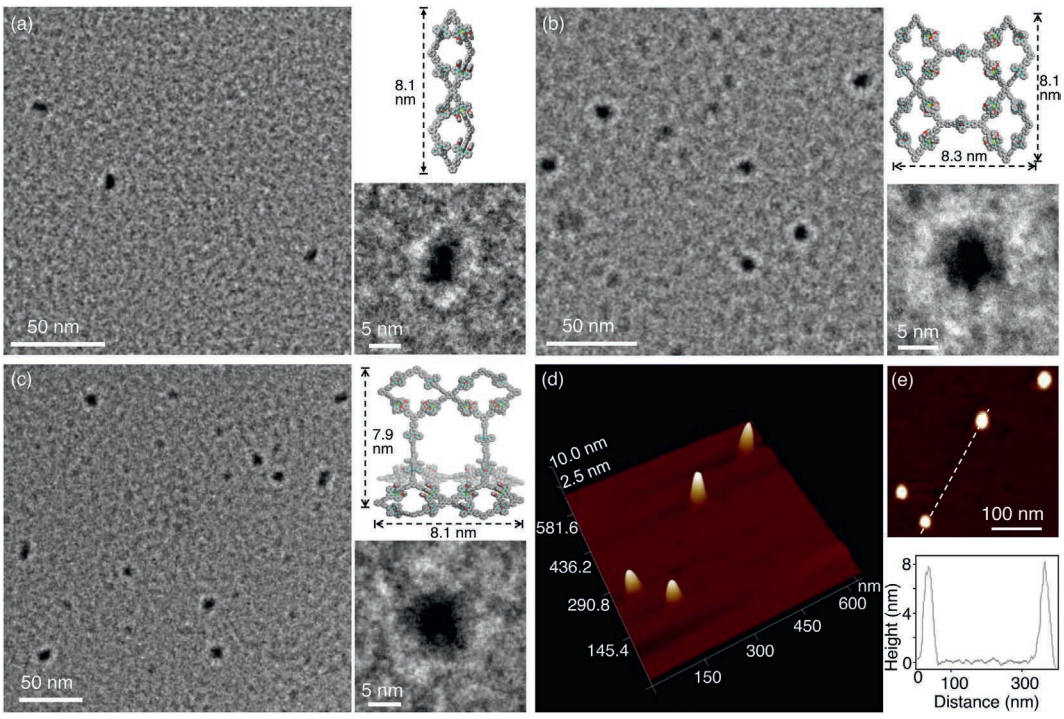


Fig. 6. TEM characterization and theoretical model of the energy-minimized structures of supramolecules (a) **R1**, (b) **R2**, and (c) **R3**; (d, e) AFM image of supramolecule **R3**.

CRediT authorship contribution statement

He Zhao: Writing – original draft, Formal analysis, Data curation, Conceptualization. **Qiangqiang Dong:** Methodology, Data curation, Conceptualization. **Fengxue Liu:** Data curation. **Ning Wang:** Data curation. **Lijun Wang:** Data curation. **Mingzhao Chen:** Methodology, Data curation. **Zhilong Jiang:** Methodology, Data curation. **Die Liu:** Supervision, Methodology. **Jun Wang:** Writing – review & editing, Methodology, Conceptualization. **Pingshan Wang:** Writing – original draft. **Yiming Li:** Writing – review & editing, Methodology, Funding acquisition, Conceptualization.

Acknowledgments

This research was supported by the Hunan Science and Technology Innovation Plan (No. 2024RC3015), the National Natural Science Foundation of China (No. 22501053), National Key Research and Development Program (Nos. 2022YFC3900902 and 2024YFC3907900), Major Science and Technology Projects of Yunnan Province (No. 202302AB080016). The authors gratefully acknowledge the Center for Advanced Research in CSU for the NMR measurements.

Supplementary materials

Supplementary material associated with this article can be found, in the online version, at doi:10.1016/j.cclet.2025.112051.

References

[1] S.R. Seidel, P.J. Stang, Acc. Chem. Res. 35 (2002) 972–983.
[2] M. Fujita, M. Tominaga, A. Hori, et al., Acc. Chem. Res. 38 (2005) 369–378.
[3] R. Chakrabarty, P.S. Mukherjee, P.J. Stang, Chem. Rev. 111 (2011) 6810–6918.
[4] H. Li, Z.J. Yao, D. Liu, et al., Coord. Chem. Rev. 293-294 (2015) 139–157.
[5] T.R. Cook, P.J. Stang, Chem. Rev. 115 (2015) 7001–7045.
[6] S. Chakraborty, G.R. Newkome, Chem. Soc. Rev. 47 (2018) 3991–4016.
[7] W.X. Gao, H.J. Feng, B.B. Guo, et al., Chem. Rev. 120 (2020) 6288–6325.
[8] X.Z. Li, C.B. Tian, Q.F. Sun, Chem. Rev. 122 (2022) 6374–6458.
[9] W. Xue, E. Benchimol, A. Walther, et al., J. Am. Chem. Soc. 146 (2024) 32730–32737.
[10] Z. Li, Y. Yan, Z. Chen, et al., CCS Chem. 7 (2025) 2381–2393.
[11] N. Han, J. Ma, H. Yu, et al., CCS Chem. 6 (2024) 1264–1277.
[12] B. Olenyuk, M.D. Levin, J.A. Whiteford, et al., J. Am. Chem. Soc. 121 (1999) 10434–10435.
[13] X. Lu, X. Li, K. Guo, et al., J. Am. Chem. Soc. 136 (2014) 18149–18155.
[14] J.F. Ayme, J.E. Beves, C.J. Campbell, et al., J. Am. Chem. Soc. 141 (2019) 3605–3612.
[15] R.G. DiNardi, A.O. Douglas, R. Tian, et al., Angew. Chem. Int. Ed. 61 (2022) e202205701.
[16] F. Su, S. Zhang, Z. Chen, et al., J. Am. Chem. Soc. 144 (2022) 16559–16571.
[17] Y. Yang, Y. Du, A.W. Heard, et al., Nat. Synth. 4 (2025) 537–551.
[18] Y. Tamaki, O. Ishitani, ACS Catal. 7 (2017) 3394–3409.
[19] M. Pan, K. Wu, J.H. Zhang, et al., Coord. Chem. Rev. 378 (2019) 333–349.
[20] Y. Xue, X. Hang, J. Ding, et al., Coord. Chem. Rev. 430 (2021) 213656.
[21] D. Xu, Y. Li, S. Yin, et al., Chem. Soc. Rev. 53 (2024) 3167–3204.
[22] H.J. Feng, L. Zeng, J.Y. Li, et al., J. Am. Chem. Soc. 146 (2024) 21791–21805.
[23] Y. Du, A. Ghosh, P.C.P. Teeuwen, et al., J. Am. Chem. Soc. 147 (2025) 20205–20211.
[24] H. Yin, J. Yuan, J. Wang, et al., Energy Environ. Sci. 18 (2025) 2231–2242.
[25] Q.F. Sun, J. Iwasa, D. Ogawa, et al., Science 328 (2010) 1144–1147.
[26] D. Fujita, Y. Ueda, S. Sato, et al., Nature 540 (2016) 563–566.
[27] Z. Zhang, Y. Li, B. Song, et al., Nat. Chem. 12 (2020) 468–474.
[28] Y. Liu, Z. Jiang, Y. Guan, et al., Cell Rep. Phys. Sci. 3 (2022) 101056.
[29] L. He, H.K. Hsu, L. Li, et al., Chem 8 (2022) 494–507.
[30] H. Zhao, A.M.S.D. Wijerathna, Q. Dong, et al., Angew. Chem. Int. Ed. 63 (2024) e202318029.
[31] W. He, Y. Yu, K. Iizuka, et al., Nat. Chem. 17 (2025) 653–662.
[32] M. Chen, J. Wang, S.C. Wang, et al., J. Am. Chem. Soc. 140 (2018) 12168–12174.
[33] X. Tan, Z. Chen, T. Liu, et al., Adv. Mater. 35 (2023) 2301096.
[34] Y. Tang, X. Zhao, Y. Li, et al., Adv. Funct. Mater. 34 (2024) 2408693.
[35] Z. Li, K. Lin, H. Fang, et al., J. Mater. Sci. Technol. 133 (2023) 249–258.
[36] T. Fukino, H. Joo, Y. Hisada, et al., Science 344 (2014) 499–504.
[37] C. Zhou, X. Li, Z. Gong, et al., Nat. Commun. 9 (2018) 807.
[38] G.L. Li, Z. Zhuo, B. Wang, et al., J. Am. Chem. Soc. 143 (2021) 10920–10929.
[39] L. Liang, W. Zhao, X.J. Yang, et al., Acc. Chem. Res. 55 (2022) 3218–3229.
[40] D. Xiao, Z. Jin, G. Sheng, et al., Nat. Chem. 16 (2024) 1906–1914.
[41] Z. Du, S. Shen, X. Su, et al., Adv. Mater. 37 (2025) 2502328.
[42] D.W. Binzel, X. Li, N. Burns, et al., Chem. Rev. 121 (2021) 7398–7467.
[43] R. Aqel, P. Severson, R. Elhajjar, Compos. Struct. 327 (2024) 117700.
[44] B. Song, S. Kandapal, J. Gu, et al., Nat. Commun. 9 (2018) 4575.
[45] H. Zhao, L. Huang, W. Liu, et al., Inorg. Chem. 63 (2024) 4152–4159.
[46] Z. Jiang, B. Chen, H. Zhao, et al., J. Am. Chem. Soc. 146 (2024) 16721–16728.
[47] S.Y. Wang, J.H. Fu, Y.P. Liang, et al., J. Am. Chem. Soc. 138 (2016) 3651–3654.
[48] J.H. Fu, S.Y. Wang, Y.S. Chen, et al., J. Am. Chem. Soc. 141 (2019) 16217–16221.
[49] G. Wang, M. Chen, J. Wang, et al., J. Am. Chem. Soc. 142 (2020) 7690–7698.
[50] J. Wang, H. Zhao, M. Chen, et al., J. Am. Chem. Soc. 142 (2020) 21691–21701.
[51] S. Perera, X. Li, M. Soler, et al., Angew. Chem. Int. Ed. 49 (2010) 6539–6544.
[52] X. Li, Y.T. Chan, M. Casiano-Maldonado, et al., Anal. Chem. 83 (2011) 6667–6674.
[53] L. Wang, B. Song, Y. Li, et al., J. Am. Chem. Soc. 142 (2020) 9809–9817.
[54] Q. Dong, F. Liu, J. Wang, et al., Angew. Chem. Int. Ed. 64 (2025) e202416327.
[55] Y.Q. Li, H. Zhao, E. Han, et al., Chem. Sci. 16 (2025) 364–370.
[56] Y.Q. Li, L. Fu, Z. Jiang, et al., Angew. Chem. Int. Ed. 64 (2025) e202503833.
[57] S. Chakraborty, W. Hong, K.J. Endres, et al., J. Am. Chem. Soc. 139 (2017) 3012–3020.
[58] H. Wang, Y. Li, H. Yu, et al., J. Am. Chem. Soc. 141 (2019) 13187–13195.
[59] G.R. Newkome, P. Wang, C.N. Moorefield, et al., Science 312 (2006) 1782–1785.
[60] T. Fukino, H. Joo, Y. Hisada, et al., Science 344 (2014) 499–504.
[61] Z. Li, M. Chen, Z. Chen, et al., J. Am. Chem. Soc. 144 (2022) 22651–22661.
[62] K. Li, W.M. Qin, W.X. Su, et al., Nat. Commun. 15 (2024) 2799.